

Extracting the orbital axis from gravitational waves of precessing binary systems

Kyohei Kawaguchi,^{1,2} Koutarou Kyutoku,^{3,4,5,2} Hiroyuki Nakano,^{6,2} and Masaru Shibata²

¹*Max Planck Institute for Gravitational Physics (Albert Einstein Institute),
Am Mühlenberg 1, Potsdam-Golm, 14476, Germany*

²*Gravitational Wave Research Center, Yukawa Institute for Theoretical Physics, Kyoto University, Kyoto 606-8502, Japan*

³*Theory Center, Institute of Particle and Nuclear Studies, KEK, Tsukuba 305-0801, Japan*

⁴*Department of Particle and Nuclear Physics, the Graduate*

University for Advanced Studies (Sokendai), Tsukuba 305-0801, Japan

⁵*Interdisciplinary Theoretical Science (iTHES) Research Group, RIKEN, Wako, Saitama 351-0198, Japan*

⁶*Faculty of Law, Ryukoku University, 67 Fukakusa Tsukamoto-cho, Fushimi-ku, Kyoto 612-8577, Japan*

(Dated: May 23, 2017)

We present a new method for extracting the instantaneous orbital axis only from gravitational wave strains of precessing binary systems observed from a particular observer direction. This method enables us to reconstruct the co-precessing frame waveforms only from observed quantities for the ideal case that the signal-to-noise ratio is high enough to analyze the waveforms directly. Specifically, we do not assume knowledge of the time evolution of the instantaneous orbital axis and the co-precessing waveforms before analyzing the data in our method. We test and measure the accuracy of our method using the numerical relativity simulation data of precessing binary black holes taken from the SXS Catalog. We show that the direction of the orbital axis is extracted within ≈ 0.02 rad error from gravitational waves emitted during the inspiral phase. The co-precessing waveforms are also reconstructed with high accuracy; the mismatch (assuming white noise) between them and the original co-precessing waveforms is typically a few times 10^{-3} including the merger-ringdown phase, and can be improved by an order of magnitude focusing only on the inspiral waveform. In this method, the co-precessing frame waveforms are not only the purely technical tools for understanding the complex nature of precessing waveforms but also direct observables.

PACS numbers: 04.30.w, 04.25.dg,

I. INTRODUCTION

The two detections (and one candidate) of gravitational waves from binary black hole mergers achieved by Advanced LIGO [4, 5, 42] have marked the beginning of the era of gravitational-wave astronomy. In particular, the first detection was achieved with significantly large signal-to-noise ratio. The information provided by the gravitational-wave observation surely enhances our knowledge about the universe, and in particular, the black holes. A number of merger events will be detected by Advanced LIGO and the following running of the other ground-based detectors, such as VIRGO [6], and KAGRA [39]. In addition, third-generation ground-base detectors, for which the sensitivity is by an order of magnitude higher than the current detectors, are proposed [35]. Furthermore, space-based detectors, such as LISA [7] and DECIGO [23], will be powerful observatories to detect massive binary black holes with significantly high signal-to-noise ratios. In the not-too-distant future, a detection of gravitational waves, for which signal-to-noise ratio is high enough for us to analyze the waveform strain data even directly without using the matched filtering method, will be achieved.

If either of the directions of two black-hole spins is not aligned with the orbital axis, the orbital precession occurs in the inspiral phase of the binary coalescence [8, 24]. Such orbital precession strongly affects the gravitational waveforms by modulating both amplitude and phase. The complex nature of the waveforms from

a precessing binary contains richer information about the binary parameters than without the orbital precession [3, 17, 25, 29]. However, the complexity also makes it difficult to understand the dependence of waveforms on the parameters.

Many efforts have been made to modeling precessing waveforms, and many frameworks have been developed to simplify those complex features [10, 11, 13–15, 19, 32, 33, 36, 37, 41]. Most remarkably, in Refs. [14, 15, 32, 36, 37], it is shown that the inspiral waveforms from a precessing binary can be dramatically simplified in the so-called “co-precessing frame”, which follows the instantaneous orbital plane of the binary. The precessing waveforms in such a frame become just as if they are from a non-precessing binary. Also, the approximate mapping between the precessing waveforms and non-precessing waveforms has been discussed [36]. Working in the co-precessing frame enables us to understand and to model the waveforms from precessing binaries much more easily than working in the inertial frame quantities. We note that, even for the case that the binary is not precessing, the modulation arises for an observer due to the mode coupling if the direction of the line of sight is misaligned with the orbital axis.

However, to extract the instantaneous orbital axis and to obtain the co-precessing frame waveforms, we need knowledge of gravitational waveforms observed from all the directions, or at least, $l = 2$ components of the spherical harmonics in the inertial frame. On the other hand, we can only obtain the strain from a particular observer

direction in real observations. Therefore, it is difficult to apply the framework of co-precessing frame directly for the observation, and hence, the co-precessing waveforms have only been treated as the intermediates for modeling the waveforms in the inertial frame.

In this paper, we present a new method for extracting the instantaneous orbital axis and for reconstructing the co-precessing frame waveforms only from gravitational wave strains observed from a particular observer direction, which can be used for the case that the signal-to-noise ratio is high enough to analyze the waveforms directly. We test and measure the accuracy of our method using the numerical relativity simulation data of the precessing binary black holes taken from SXS Catalog [1, 20, 30, 31]. In our method, knowledge of the time evolution of the instantaneous orbital axis and the co-precessing waveforms are not assumed before analyzing the data, and thus, the method can also be used for the case that the time evolution does not obey the prediction of general relativity. Our method is composed of two basic ideas: One is the transformation, which we call the mode decomposition, that decomposes the wave strain into Fourier(-like) components in terms of the harmonic modes in the co-precessing frame rather than the frequency. The other is the procedure to extract the ‘‘orbital phase’’ of the binary for use in the mode decomposition only from the precessing wave strain.

Before moving to the explanation of our method, we summarize conventions and basic assumption which we employ in this paper. Through out this paper, we employ the geometrical units $c = G = 1$, where c and G are the speed of light and the gravitational constant, respectively. We refer to the total mass of the system at the infinite separation as M . Among several definitions for the co-precessing frame [15, 32, 36, 37], in this paper, we employ the so-called quadrupole-preferred frame (referred to as the quadrupole-aligned (QA) frame or the QA method in the following) introduced in Refs. [36, 37]. We refer to z -axis obtained by the quadrupole-preferred frame as the direction of the orbital angular momentum or the instantaneous orbital axis, $\hat{\mathbf{L}}$ ($|\hat{\mathbf{L}}| = 1$), just for simplicity. We note that $\hat{\mathbf{L}}$ does not always agree with and rather slightly deviates from the Newtonian orbital angular momentum, $\hat{\mathbf{L}}_N$, defined in Refs. [15, 24] due to the higher order post-Newtonian corrections.

To describe the precession of the binary, we introduce a coordinate system as follows. First, we describe the direction of the source in the sky by two polar angles, θ and ϕ , and define a unit vector, $\hat{\mathbf{N}}$, as the direction from the source to the observer. Next, we introduce two bases in the plane perpendicular to $\hat{\mathbf{N}}$, $\hat{\boldsymbol{\theta}}$ and $\hat{\boldsymbol{\phi}}$, which are the unit vectors in the directions of $(\partial/\partial\theta)^i$ and $(\partial/\partial\phi)^i$, respectively. Then, we introduce a Cartesian coordinate system, (x, y, z) , in the source frame in such a way that x, y , and z directions agree with $\hat{\boldsymbol{\phi}}, \hat{\boldsymbol{\theta}}$, and $\hat{\mathbf{N}}$, respectively (see Fig. 1). We describe the direction of the orbital angular momentum, $\hat{\mathbf{L}}(t)$, by introducing two polar angles,

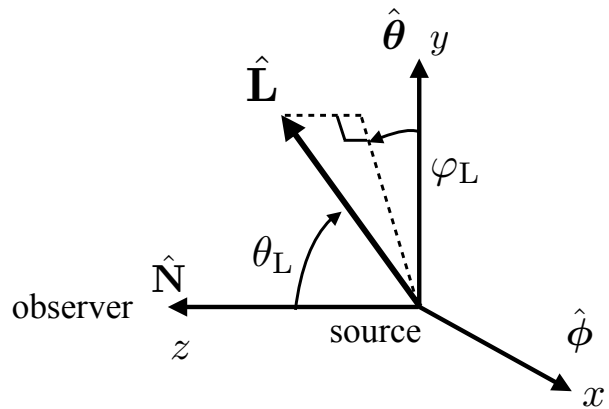


FIG. 1. The definitions of the angles in the source frame. The unit vector, $\hat{\mathbf{N}}$, denotes the direction from the source to the observer. $\hat{\boldsymbol{\theta}}$ and $\hat{\boldsymbol{\phi}}$ denote unit vectors in the directions of $(\partial/\partial\theta)^i$ and $(\partial/\partial\phi)^i$, respectively, where those two angles describe the sky position of the source.

$\theta_L(t)$ and $\varphi_L(t)$, in the source frame defined by

$$\theta_L(t) = \cos^{-1} \left[\hat{L}_z(t) \right], \quad (1)$$

$$\varphi_L(t) = \text{Arg} \left[\hat{L}_x(t) + i\hat{L}_y(t) \right] - \frac{\pi}{2}, \quad (2)$$

where \hat{L}_i ($i = x, y, z$) is a component of $\hat{\mathbf{L}}$ in the source frame. We note that we shift φ_L by $-\pi/2$ so that $\hat{\mathbf{L}}$ lies in yz -plane for the case $\varphi_L = 0$.

We denote a complex waveform strain by $h = h_+ - ih_\times$, where h_+ and h_\times are the plus and cross modes of gravitational-wave polarization defined by

$$h_+ = \frac{1}{2} \left(h_{\hat{\boldsymbol{\theta}}\hat{\boldsymbol{\theta}}}^{\text{TT}} - h_{\hat{\boldsymbol{\phi}}\hat{\boldsymbol{\phi}}}^{\text{TT}} \right), \quad (3)$$

$$h_\times = -h_{\hat{\boldsymbol{\theta}}\hat{\boldsymbol{\phi}}}^{\text{TT}}. \quad (4)$$

Here, h_{ij}^{TT} is a transverse-traceless component of the metric perturbation. We note that the sign of h_\times is opposite from the usual definition due to our different choice of the coordinate system.

In this paper, we focus only on the case that the complex waveform strain, h , is known and do not consider the effect of the noise to demonstrate the potential of our method. Using ground-based detectors, multiple detectors are needed to determine h . The sky localization of the event is also important to determine h accurately. The follow-up observations of electromagnetic counterparts will help for determining the sky location of the events including neutron stars [18]. In the observations of binary black holes by space-based detectors such as LISA and DECIGO, our method will be useful because they could determine the sky position accurately [26, 40]. We leave the study how the errors in the observation influence the accuracy for extracting the orbital axis in our

method in future study. We also note that, in this paper, our method is only tested for the data of precessing binary black holes for which the precessing time scale is always much longer than their orbital period except just before the mergers.

II. METHOD

A. Mode decomposition

The waveforms from a precessing binary observed in the inertial frame can be described by using precessing-frame waveforms as [36, 37],

$$h(t) = \sum_{l=2}^{\infty} \sum_{m=-l}^l e^{-2i\varphi_L(t)} {}_{-2}Y_m^l[-\theta_L(t), -\psi_L(t)] h_{lm}^{\text{QA}}(t), \quad (5)$$

where ${}_{-2}Y_m^l$ is the spin-weighted spherical harmonics, $h_{lm}^{\text{QA}}(t)$ is the (l, m) mode in the co-precessing frame, and $\psi_L(t)$ is the angle defined by

$$\psi_L(t) = - \int_0^t \dot{\varphi}_L(t') \cos \theta_L(t') dt', \quad (6)$$

which comes from the minimal rotation condition of co-precessing frame [14]. The initial value of ψ_L can be chosen arbitrarily, and we set it to be zero in this work. Here, we assume that the time scales of the orbital precession and the gravitational-radiation reaction are much longer than the orbital period. Then, as the waveforms in the co-precessing frame have similar features to non-precessing waveforms, we can assume that for any values of l and m , h_{lm}^{QA} can be decomposed into slowly evolving amplitude part, $A_{lm}^{\text{QA}}(t)$ and rapidly evolving phase part, $e^{-im\Phi^{\text{QA}}(t)}$. Here, $\Phi^{\text{QA}}(t)$ is the orbital phase of the binary defined by the half of the phase of $(l, m) = (2, 2)$ mode in the co-precessing frame. We note that $\Phi^{\text{QA}}(t)$ is slightly different from the orbital phase in the standard post-Newtonian framework which is defined with respect to the relative coordinate separation of the binary (see Ref. [9]). Then, we can rewrite Eq. (5) as

$$h(t) \approx \sum_{l=2}^{\infty} \sum_{m=-l}^l e^{-2i\varphi_L(t)} {}_{-2}Y_m^l[-\theta_L(t), 0] A_{lm}^{\text{QA}}(t) \times e^{-im[\Phi^{\text{QA}}(t) + \psi_L(t)]}. \quad (7)$$

Equation (7) shows that the waveforms in the inertial frame can be described by the superposition of the wave components for which the phase is $-m\Phi(t) = -m[\Phi^{\text{QA}}(t) + \psi_L(t)]$, with relatively slowly evolving part of $e^{-2i\varphi_L(t)} {}_{-2}Y_m^l[-\theta_L(t), 0] A_{lm}^{\text{QA}}(t)$. In particular,

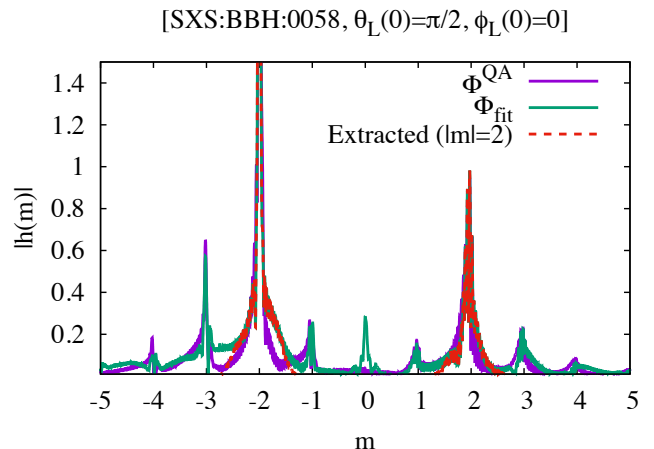


FIG. 2. The mode spectra of the gravitational waveforms from a precessing binary (SXS:BBH:0058). We used the waveforms observed from the direction in which $\theta_L = \pi/2$ and $\varphi_L = 0$ are satisfied at the initial time of the simulation. The curves “ Φ^{QA} ” and “ Φ_{fit} ” show the mode spectra using Φ^{QA} and Φ_{fit} as the orbital phase, respectively. The curve “Extracted ($|m|=2$)” shows the mode spectra to which a window function Eq. (15) is applied.

the dominant modes of gravitational waves are contained in the wave components with $(l, m) = (2, \pm 2)$.

If $\Phi(t)$ is known a priori, we can decompose each wave component in Eq. (7) by performing a transformation as

$$\tilde{h}(m) = \int_{-\infty}^{\infty} h(t) e^{-im\Phi(t)} \dot{\Phi}(t) dt. \quad (8)$$

This transformation, which we refer to as the *mode decomposition* in the following, is the Fourier transformation of h not with respect to time but with respect to the phase Φ . We note that there is a degree of freedom in the choice of the phase variable for the mode decomposition, for which the choice is non-trivial in real observations. For example, we can use $\Phi + \varphi_L$ as the phase variable. Therefore, $\tilde{h}(m)$ has ambiguity in its definition.

We can easily reconstruct the time-domain waveforms by the inverse transformation,

$$h(t) = \frac{1}{2\pi} \int_{-\infty}^{\infty} \tilde{h}(m) e^{im\Phi(t)} dm. \quad (9)$$

We note that $h(t)$ does not have any ambiguity associated with the complex phase of $\tilde{h}(m)$ mentioned above.

As an illustration, we perform the mode decomposition of precessing waveforms using the waveforms derived in numerical relativity simulations. At a first sample, we employ SXS:BBH:0058 in Refs. [1, 30, 31], which is a waveform of a binary black hole for the case that the mass ratio is 5, only the larger mass black hole has a dimensionless spin with 0.5, and the black-hole spin initially lies in the orbital plane. We generate the complex

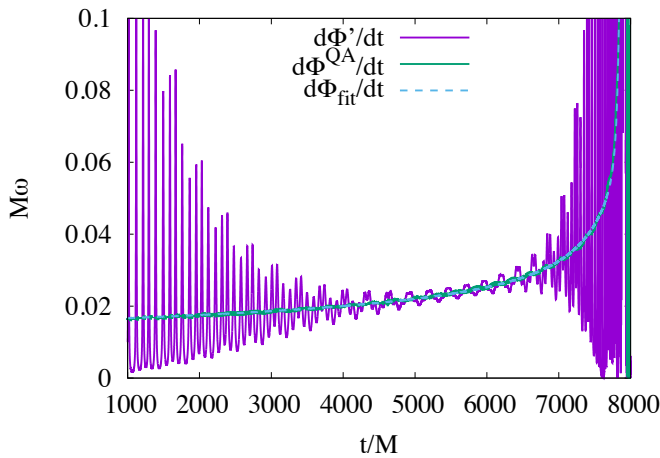


FIG. 3. The comparison of orbital frequencies obtained by several methods. The curves “ $d\Phi'/dt$ ”, “ $d\Phi^{QA}/dt$ ”, and “ $d\Phi_{\text{fit}}/dt$ ” show orbital frequencies obtained by the time derivative of Φ' , Φ^{QA} , and Φ_{fit} , respectively.

waveform strain observed from a specific direction by employing all the components of spherical harmonics up to $l = 8$. In this section, we specifically choose the direction that satisfies $\theta_L = \pi/2$ and $\varphi_L = 0$ at the initial time of the simulation. The results for different directions are shown in Sec. III. We use $\Phi^{QA}(t)$ as the phase variable for performing the mode decomposition.

Figure 2 plots the resulting mode spectrum (see the plot referred to as Φ_{QA}). This shows that the mode spectrum has peaks at integer values of m , and each peak is clearly separated. This suggests that we can approximately extract m -mode wave components of h by performing the mode decomposition Eq. (8). Then, applying an appropriate filter or window function to the mode spectrum $\hat{h}(m)$, it is possible to approximately reconstruct the time-domain waveforms by Eq. (9) (see Sec. II C).

B. Extracting the orbital phase

To practically perform the mode decomposition of the observed waveforms, we need to extract the orbital phase of the binary from the observational data. If the binary is not precessing and the observer is located along the orbital axis, the orbital phase of the binary in the inspiral orbits can be extracted from the waveforms by

$$\Phi'(t) = \frac{1}{2} \int_0^t \frac{\left| \text{Im} \left[h^*(t') \dot{h}(t') \right] \right|}{|h(t')|^2} dt', \quad (10)$$

where h^* denotes the complex conjugate of h . However, if the binary is precessing, we cannot obtain the orbital phase directly from Eq. (10). In Fig. 3, we plot the time derivative of $\Phi'(t)$ calculated by Eq. (10) as well as that

of Φ^{QA} for the same waveforms as those used in Fig. 2. We find that $\Phi'(t)$ is strongly oscillating due to the mixing of wave components with different frequencies, while $\dot{\Phi}^{QA}(t)$ evolves monotonically. Therefore, we cannot use $\Phi'(t)$ directly for the mode decomposition.

Instead of employing $\Phi'(t)$, we have to extract the non-oscillatory part of $\Phi'(t)$ for the mode decomposition. While $\Phi'(t)$ oscillates strongly, it still behaves in a similar manner to $\Phi^{QA}(t)$ if we take the time average. Therefore, we expect that we can approximately extract the “orbital phase” which can be used for the mode decomposition if we remove the oscillation from $\Phi'(t)$. In this work, we extract the non-oscillatory part by fitting $\Phi'(t)$ with a non-oscillating function defined by

$$\Phi_{\text{fit}}(t) = \begin{cases} \Phi_{\text{fit}}^{\text{ins}}(t) & t \leq t_0, \\ b_0 + c_1(t - t_0) + b_1 \left[e^{-(t-t_0)/c_2} - 1 \right] & t \geq t_0, \end{cases} \quad (11)$$

where $\Phi_{\text{fit}}^{\text{ins}}(t)$ is the inspiral part defined by

$$\begin{aligned} \Phi_{\text{fit}}^{\text{ins}}(t) = & a + a_1(t_1 - t)^{5/8} + a_2(t_1 - t)^{3/8} \\ & + a_3(t_1 - t)^{1/4} + a_4(t_1 - t)^{1/8} + a_5^{(1)} \ln(t_1 - t) \\ & + \left[a_6^{(0)} + a_6^{(1)} \ln(t_1 - t) \right] (t_1 - t)^{-1/8} \\ & + a_7(t_1 - t)^{-1/4}. \end{aligned} \quad (12)$$

Here, the functional form of Eq. (12) is motivated by Taylor-T3 approximant [12, 16]. For this prescription, t_0 is taken to be the time of global maximum of $|h(t)|$ ($t_0 = 7857M$ for this case), and b_0 and b_1 are chosen so that $\Phi_{\text{fit}}(t)$ and $\dot{\Phi}_{\text{fit}}(t)$ are continuous at $t = t_0$. We determine a_n ($n = 1, \dots, 7$), c_1 , c_2 and $t_1 > t_0$ by the least-square fitting method using $\Phi'(t)$. We only use the data from $t = 1000M$ ($t = 0$ is the time at which the simulation starts) to the time that $|h(t)|$ becomes smaller than 5% of its peak value for the first time. This time window is chosen to avoid the unphysical modulation in the beginning of the simulation and the unimportant part of the waveforms after the onset of merger.

In Fig. 3, we plot $\dot{\Phi}_{\text{fit}}(t)$. We find that $\dot{\Phi}_{\text{fit}}$ agrees with $\dot{\Phi}^{QA}(t)$ within 2%. We also plot the mode spectrum of the waveform using $\Phi_{\text{fit}}(t)$ in Fig. 2. Though there is slight deviation from the ones obtained using $\Phi^{QA}(t)$, we find that the mode spectrum has peaks in integer values of m and each peak is clearly separated. This suggests that $\Phi_{\text{fit}}(t)$ can be a good substitute for $\Phi^{QA}(t)$ to perform the mode decomposition. We note that $\dot{\Phi}_{\text{fit}}(t)$ does not strictly agree with neither $\dot{\Phi}(t)$ nor $\dot{\Phi}^{QA}(t)$, but rather agrees well with $\dot{\Phi}(t) + \dot{\varphi}_L(t) \text{sign}[\cos \theta_L(t)]$. We can also prove this analytically by assuming that $(l, m) = (2, \pm 2)$ modes in the co-precessing frame are the dominant modes. Because $|\dot{\varphi}_L|$ is much smaller than $|\dot{\Phi}(t)|$, the deviation of $\Phi_{\text{fit}}(t)$ from $\Phi(t)$ only weakly affect the accuracy of the mode decomposition at least for extracting the dominant modes in the inspiral orbits.

C. Extracting the wave components

We introduce here a window function to extract specific wave components in the mode spectra. We define a one-sided amplitude of the mode spectra by

$$A(m) := \sqrt{|\tilde{h}(m)|^2 + |\tilde{h}(-m)|^2}. \quad (13)$$

$A(m)$ has the largest peak in $|m| \approx 2$, and small side peaks in integer values of m . As we mentioned above, the information of the dominant modes of gravitational waves is contained primarily in the modes of $|m| = 2$. To single out only the information around $|m| \approx 2$, we performed the extraction in following three steps. First, we fit $A(m)$ around $|m| \approx 2$ by a Lorentzian function,

$$L(m; A_0, m_p, m_{1/2}) = \frac{A_0}{1 + (m - m_p)^2/m_{1/2}^2}, \quad (14)$$

where A_0 is the peak amplitude, m_p and $m_{1/2}$ are the location of the peak and the half-width at half maximum, respectively. We perform the least-square fitting to determine these fitting parameters. We note that m_p is also a fitting parameter, while its initial guess is set to be 2. We find that the value after the fitting deviates from the initial value only by ≈ 0.02 .

Next, we introduce a window function $w(m)$ defined by

$$w(m) = \begin{cases} 1 & |m - m_p| < \Delta m_1, \\ H(m) + [1 - H(m)] \frac{L(m)}{A(m)} & \Delta m_1 \leq |m - m_p| < \Delta m_2, \\ \frac{L(m)}{A(m)} & \Delta m_2 \leq |m - m_p|, \end{cases} \quad (15)$$

where

$$H(m) = \frac{1}{2} \left[1 + \cos \left(\pi \frac{|m - m_p| - \Delta m_1}{\Delta m_2 - \Delta m_1} \right) \right]. \quad (16)$$

Here, we chose $\Delta m_1 = 0.35$ and $\Delta m_2 = 0.75$. Finally, we define the extracted mode spectrum $\tilde{h}^{\text{ext}}(m)$ by $\tilde{h}^{\text{ext}}(m) = w(m) \tilde{h}(m)$.

Applying this window function, the amplitude of the mode spectra in $|m - m_p| > \Delta m_1$ is continuously suppressed and normalized to $L(m)$, and the peaks in $|m| \neq 2$ are suppressed. Indeed, a plot for the extracted mode spectrum, $\tilde{h}^{\text{ext}}(m)$, in Fig. 2 shows that only the peaks in $|m| = 2$ are remaining. We can then obtain the wave components for $m = 2$ and -2 in the time domain, $h_{m=2}^{\text{ext}}(t)$ and $h_{m=-2}^{\text{ext}}(t)$, by performing the inverse transformation of the spectra for each peak using $\Phi_{\text{fit}}(t)$. Figure 4 compares the original and extracted waveforms in the time domain. The original waveforms and sum of $m = \pm 2$ wave components agree approximately with

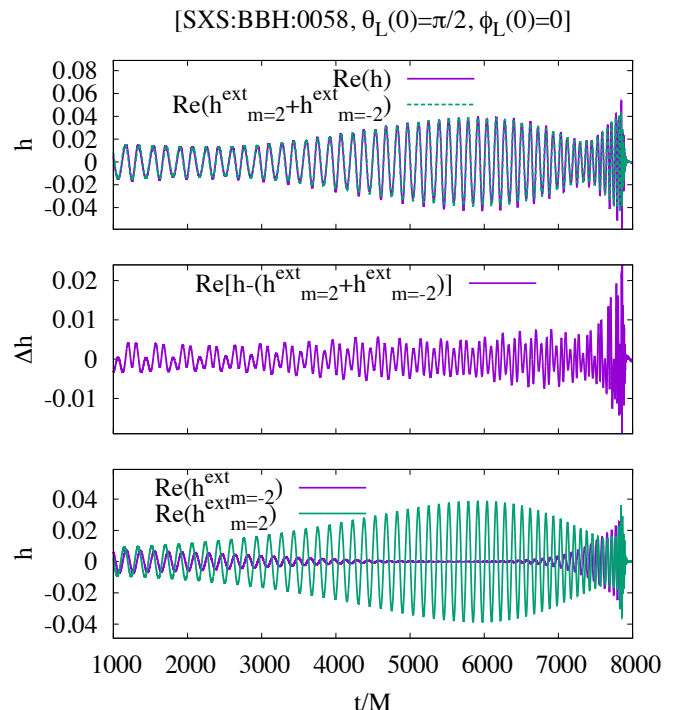


FIG. 4. The comparison of the original and extracted waveforms in the time domain. The upper panel shows the real part of the original complex waveform strain, h , and sum of $m = \pm 2$ wave components extracted from the mode spectrum with respect to $\Phi_{\text{fit}}(t)$, and the middle panel shows the difference between those two waveforms. The bottom panel shows the real part of $m = 2$ and $m = -2$ mode wave components.

each other (see the upper panel in Fig. 4), and the difference between these two waveforms oscillates in different frequency to the dominant-mode frequency (see the middle panel in Fig. 4). This suggests that wave components of $m \neq \pm 2$ are removed and only dominant wave components are extracted from the original strain. The bottom panel in Fig. 4 shows the real part of $m = 2$ and $m = -2$ mode wave components. The smooth change in the amplitude reflects the orbital precession (see Eq. (17)).

D. Extracting the instantaneous orbital axis

Assuming that the extracted wave components of $|m| = 2$ are dominated by the $l = 2$ components of the spherical harmonics, we can describe each wave component by

$$h_{m=\pm 2}^{\text{ext}}(t) \approx \frac{1}{8} \sqrt{\frac{5}{\pi}} [1 \pm \cos \theta_L(t)]^2 A_{22}^{\text{QA}}(t) e^{-2i[\varphi_L(t) \pm \Phi(t)]}. \quad (17)$$

If we further assume that the system has an approxi-

III. APPLICATION

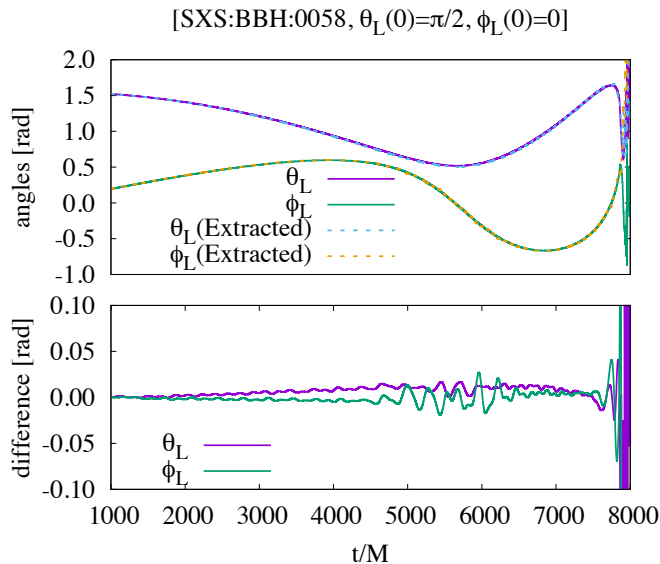


FIG. 5. The comparison of θ_L and φ_L obtained from the original QA method and the ones obtained from the extraction procedure using the mode decomposition.

mate equatorial symmetry in the co-precessing frame¹, and hence, $A_{22}^{\text{QA}}(t) = A_{2-2}^{\text{QA}}(t)$ holds, we can measure $\theta_L(t)$, $\varphi_L(t)$, and $\Phi(t)$ by

$$\theta_L(t) = \cos^{-1} \left[\frac{\sqrt{|h_{m=2}^{\text{ext}}(t)|} - \sqrt{|h_{m=-2}^{\text{ext}}(t)|}}{\sqrt{|h_{m=2}^{\text{ext}}(t)|} + \sqrt{|h_{m=-2}^{\text{ext}}(t)|}} \right], \quad (18)$$

$$e^{-4i\varphi_L(t)} = \frac{h_{m=2}^{\text{ext}}(t) h_{m=-2}^{\text{ext}}(t)}{|h_{m=2}^{\text{ext}}(t)| |h_{m=-2}^{\text{ext}}(t)|}, \quad (19)$$

and

$$e^{-4i\Phi(t)} = \frac{h_{m=2}^{\text{ext}}(t) h_{m=-2}^{\text{ext},*}(t)}{|h_{m=2}^{\text{ext}}(t)| |h_{m=-2}^{\text{ext}}(t)|}. \quad (20)$$

$\Phi^{\text{QA}}(t)$ is determined from $\Phi(t)$ and $\psi_L(t)$, where $\psi_L(t)$ is determined by Eq. (6) using the extracted result of $\theta_L(t)$ and $\varphi_L(t)$ (note that $\varphi_L(t)$ is only determined up to multiple times $\pi/2$ in our method). Using $\theta_L(t)$, we can determine $A_{22}^{\text{QA}}(t)$ (or $A_{2-2}^{\text{QA}}(t)$) from $\sqrt{|h_{m=2}^{\text{ext}}(t)|}$ (or $\sqrt{|h_{m=-2}^{\text{ext}}(t)|}$). Then, the $(l, m) = (2, \pm 2)$ modes in the co-precessing frame are reconstructed by $A_{2\pm 2}^{\text{QA}}(t) e^{\mp 2i\Phi^{\text{QA}}(t)}$.

In this section, we test the extraction method introduced in the previous section. First, we use the waveform strain generated from the data of SXS:BBH:0058, which was also used in Figs. 2 and 3. Figure 5 shows the comparisons of $\theta_L(t)$ and $\varphi_L(t)$ obtained from the original QA method and the ones obtained from the extraction procedure using the mode decomposition. In the figure, we find that $\theta_L(t)$ and $\varphi_L(t)$ agree well between two methods, and we find the deviations are always smaller than 0.03 rad until $t \approx 7700 M$.

Next, we check how accurately the reconstruction of the co-precessing waveforms works. We compare the $(l, m) = (2, 2)$ mode in the co-precessing frame obtained by the original QA method and the ones reconstructed by our method. Here, instead of using the QA waveforms directly, we take the average of the $(l, m) = (2, \pm 2)$ modes, namely, $\bar{h}_{22}^{\text{QA}} = (h_{22}^{\text{QA}} + h_{2-2}^{\text{QA},*})/2$ for the QA method. This average is taken so that the equatorial symmetry in the co-precessing frame is imposed. This is consistent with the assumption which we made in the extraction procedure. In addition, this removes most parts of the residual modulations in h_{22}^{QA} and h_{2-2}^{QA} which remain even after taking the co-precessing frame [11, 13]. Since these modulations, for which the oscillation frequency is different from the dominant mode, are expected to be removed by the extraction procedure, it is natural to use the averaged waveforms.

In the top and middle panels in Fig. 6, we compare the co-precessing frame amplitude by the two methods and show the phase difference between two waveforms, respectively. The two waveforms agree well with each other in both amplitude and the phase until $t \approx 7700 M$. Their deviations are found to become large in $t = 7700$ – $8000 M$, while the deviation in the phase keeps smaller than ≈ 0.5 rad until the peak amplitude is reached. This late-time deviation is also found in the comparisons of $\theta_L(t)$ and $\varphi_L(t)$. We suspect that these deviations would be due to the fact that the precession timescale becomes short and become comparable to the orbital period just before the merger. If we perform the mode decomposition focusing only on the waveforms after $t \approx 7700 M$, the spreads of the peaks in the spectra become broad and overlap with each other as two time scales become comparable. This suggests that some part of information in the merger-ringdown stages leaks to the other peaks in the spectra. The prescriptions for the phase fitting in Eq. (11) and the window function in Eq. (15) can also be the source for the errors. If so, further improvement is needed for these forms. We leave the further investigation for the origin of their errors as the future task.

To discuss the agreements of the waveforms more quantitatively, we define the mismatch between two complex

¹ Strictly speaking, this is not true as Ref. [13] has pointed out that there remains some asymmetric modulation in the waveforms even in the co-precessing frame.

waveform strains, h_1 and h_2 , by

$$\mathcal{M}(h_1, h_2) = 1 - \max_{\varphi_c} \frac{\text{Re} [(h_1|h_2 e^{i\varphi_c})]}{\sqrt{(h_1|h_1)}\sqrt{(h_2|h_2)}}, \quad (21)$$

where $(\cdot|\cdot)$ is the Hermitian inner product defined by

$$(h_1|h_2) = \int_{t_i}^{t_f} h_1^*(t) h_2(t) dt. \quad (22)$$

Here, t_i is the lower bound of the integral which is always set to be $1000 M$ in this work, and t_f is the upper bound of the integral. We note that our definition of the mismatch is different from the usual one that is employed in previous data-analysis studies (see, e.g., Ref. [11]). Our definition is identical with the usual one for the case that the noise spectrum density of the detector is assumed to be white [36]. We employ the definition in Eqs. (21) and (22) in this paper because we can calculate the mismatch in the time domain and easily show in which part of the waveforms the error is induced. We find that mismatches calculated by Eqs. (21) and (22) for $(t_i, t_f) = (1000 M, \infty)$ are similar to the values calculated by the usual definition of mismatch assuming $M = 10 M_\odot$ and using a designed noise curve of Advanced LIGO (for the zero tuned high power configuration [2]).

In the bottom panel of Fig. 6, we plot the mismatch between the two waveforms as a function of the upper bound of integral, t_f . We find that the mismatch is always below 10^{-4} until the time of peak amplitude, and rapidly increases to the order of 10^{-3} after the peak time. This shows that the reconstructed waveforms have the largest error around the time of peak amplitude.

To further show the usefulness of our method for a variety of precessing binaries, we calculate the mismatches of the co-precessing $(l, m) = (2, 2)$ mode between those obtained by the QA method and by the mode decomposition method, picking up three precessing binary black hole models. We employ SXS:BBH:0058, SXS:BBH:0037, and SXS:BBH:0164 in SXS Catalog [1, 20, 30, 31], and for each model, we generate five complex waveform strains observed from five different inclinations. We again set $t_i = 1000 M$ for computing the mismatches. We compute two mismatches for each model adopting different upper bound of the integral t_f . One is computed by setting t_f to be infinity, and the other is by setting t_f to be the time earlier by $100 M$ than the peak of amplitude. The parameters of the models, the inclination of the observers, and the calculated mismatches are summarized in Table I.

For every waveform strain derived from SXS:BBH:0058, mismatches are always a few times 10^{-3} for the case that the ringdown waveforms are included ($(t_i, t_f) = (1000 M, \infty)$). Mismatches decrease by an order of magnitude by excluding the waveforms in the merger and ringdown stages ($(t_i, t_f) = (1000 M, t_0 - 100 M)$). Hence, the error of the reconstructed co-precessing frame waveforms is primarily

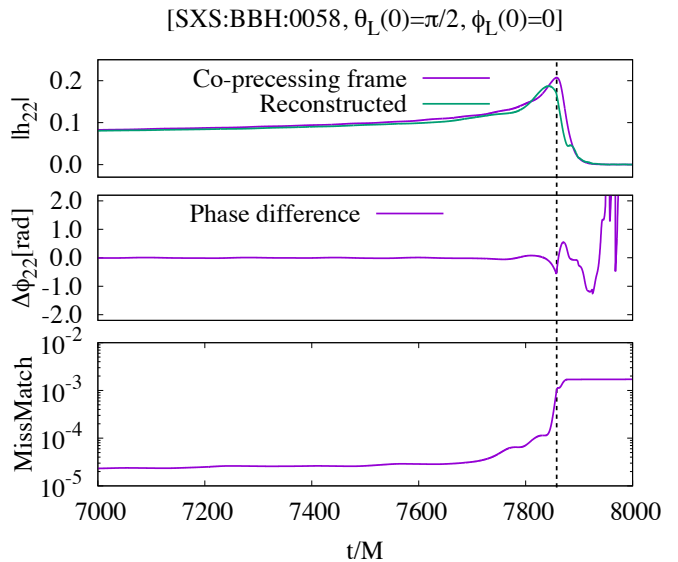


FIG. 6. The comparison of the co-precessing frame waveforms obtained by the QA method and the ones reconstructed from extracted waveforms using the mode decomposition. The top panel compares of the co-precessing frame amplitude of the $(l, m) = (2, 2)$ mode. The middle panel shows the phase difference between two waveforms for the case that the mismatch for $(t_i, t_f) = (1000 M, \infty)$ is the minimum (see Eq. (21)). The bottom panel shows the mismatch between the two waveforms as a function of the upper bound of integral, t_f . The lower band of the integral, t_i , is always set to be $1000 M$. We note that we take the average of the $(l, m) = (2, \pm 2)$ modes for the QA waveforms to impose the equatorial symmetry. The vertical dashed line denotes the peak time of the amplitude.

accumulated in the merger and ringdown stages, as has already been found in Fig. 6.

For SXS:BBH:0037 and SXS:BBH:0164, the features of mismatches are quite similar to those of SXS:BBH:0058. In particular, the result for SXS:BBH:0164 shows that our extraction method can be useful not only for single-spinning binary black holes but also for double-spinning binaries. However, for $\theta_L(0) = 0, \pi/4$ and π of SXS:BBH:0037 and $\theta_L(0) = 0$ and π of SXS:BBH:0058, we find that the mismatches are worse than the other cases. In particular, the improvement of mismatches by excluding the merger and ringdown stages is not as remarkable as for the other cases. This suggests that the reconstructed waveforms have errors not only in the merger and ringdown stages but also in the inspiral stage for these cases. One possible source of these errors is induced when extracting $\varphi_L(t)$ from the waveform strain. As is seen in Eq. (17), the norms of $h_{m=-2}^{\text{ext}}$ and $h_{m=2}^{\text{ext}}$ become close to zero for the case that $\theta_L(t)$ close to 0 and π (i.e., the line of sight agrees with the orbital axis), respectively. In such cases, the extraction of $\varphi_L(t)$ becomes quite sensitive to the error in $h_{m=\pm 2}^{\text{ext}}$. Indeed, it is shown in Fig. 7 that $\varphi_L(t)$ has a large error at which

Model	$\theta_L(0)$	\mathcal{M}		
		$t_i = 1000 M$ $t_f = \infty$	$t_i = 1000 M$ $t_f = t_0 - 100 M$	
SXS:BBH:0058	0	1.13×10^{-3}	2.13×10^{-4}	
	$\pi/4$	1.40×10^{-3}	1.66×10^{-4}	
	$m_1/m_2 = 5$	$\pi/2$	1.71×10^{-3}	5.58×10^{-5}
	$\mathbf{S}_1 = (0.5, 0, 0)$	$3\pi/4$	2.54×10^{-3}	1.81×10^{-4}
	$\mathbf{S}_2 = \mathbf{0}$	π	1.02×10^{-3}	1.19×10^{-4}
SXS:BBH:0037	0	4.05×10^{-3}	1.11×10^{-3}	
	$\pi/4$	5.93×10^{-3}	5.03×10^{-3}	
	$m_1/m_2 = 3$	$\pi/2$	1.32×10^{-3}	8.36×10^{-5}
	$\mathbf{S}_1 = (0.5, 0, 0)$	$3\pi/4$	1.81×10^{-3}	2.31×10^{-4}
	$\mathbf{S}_2 = \mathbf{0}$	π	9.18×10^{-3}	2.95×10^{-3}
SXS:BBH:0164	0	6.94×10^{-3}	5.73×10^{-3}	
	$\pi/4$	2.42×10^{-3}	5.56×10^{-4}	
	$m_1/m_2 = 1$	$\pi/2$	1.35×10^{-3}	8.41×10^{-5}
	$\mathbf{S}_1 = \mathbf{S}_2$	$3\pi/4$	3.17×10^{-4}	1.31×10^{-5}
	$= (0.52, 0, 0.3)$	π	6.93×10^{-3}	5.72×10^{-3}

TABLE I. The list of the mismatch between the $(l, m) = (2, 2)$ mode in the co-precessing frame obtained by the original QA method and the one obtained by our method. The first left column shows the model names in SXS Catalog [1, 20, 30, 31] as well as their mass ratios and their black-hole spins. The numbers in the brackets describes the x , y , and z components of the black-hole spin in the source frame with $\theta_L = 0$ and $\varphi_L = 0$. The second left column shows the initial values of θ_L , which describe the initial direction of the observer with respect to the orbital axis. Here, we chose the observer so that the initial values of φ_L are always set to be 0. The third and fourth columns show the mismatches employing $(t_i, t_f) = (1000 M, \infty)$ and $(t_i, t_f) = (1000 M, t_0 - 100 M)$, respectively. We note that our definition of the mismatch is different from the usual one that is employed in previous data-analysis studies (see the sentences below Eq. (22)).

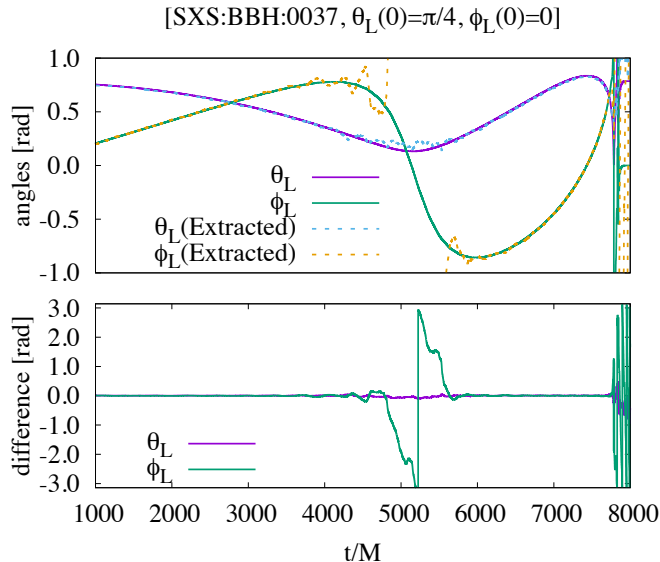


FIG. 7. The same as Fig. 5 but for $\theta_L(0) = \pi/4$ of SXS:BBH:0037. For the comparison, we shift the extracted result of φ_L by $\pi/2$ and restrict its value to $[-\pi, \pi]$ due to its uncertainty in the extraction (see Eq. (19)).

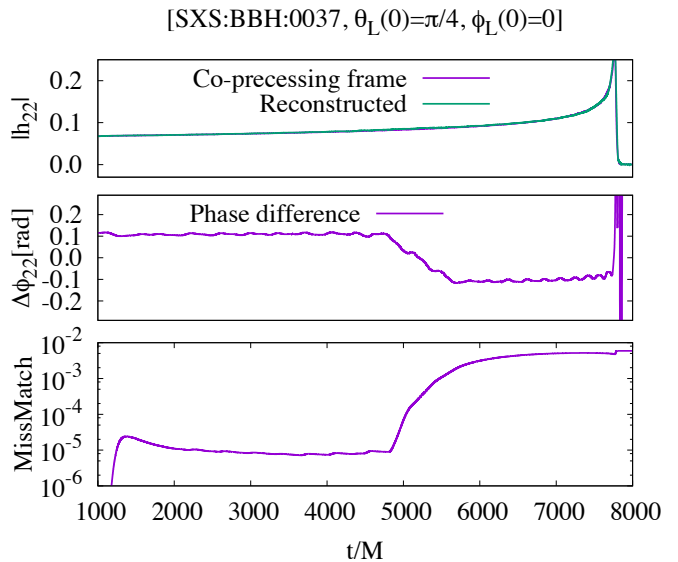


FIG. 8. The same as Fig. 6 but for $\theta_L(0) = \pi/4$ of SXS:BBH:0037.

$\theta_L(t)$ passes by 0. $\Phi(t)$ also suffers from the error for the same reason (see Eq. (20)). Therefore, the match can be deteriorated if $\theta_L(t)$ passes by 0 or π . In fact, in the extracted data in $\theta_L(0) = 0, \pi/4$ and π of SXS:BBH:0037 and $\theta_L(0) = 0$ and π of SXS:BBH:0164, we find that there is some interval that $\theta_L(t)$ passes by 0 or π during its evolution, and the phase error relative to the QA method increases during this period (see Figs. 7 and 8).

Fortunately, the error in Φ^{QA} would be much smaller than the errors in $\varphi_L(t)$ and $\Phi(t)$ because these errors are canceled out by taking the combination. For example, for the case that $\theta_L(t)$ is close to 0, $\dot{\Phi}^{\text{QA}}(t)$ is approximately written as $\dot{\Phi}(t) + \dot{\varphi}_L(t)$ using Eq. (6). On the other hand, $\Phi(t) + \varphi_L(t)$ is determined only from argument of $h_{m=2}^{\text{ext}}(t)$. Since $h_{m=2}^{\text{ext}}(t)$ contains the main source of the error in this situation, $\Phi^{\text{QA}}(t)$ is expected to have smaller error than $\varphi_L(t)$ or $\Phi(t)$. However, as is found in Fig. 8, some error still remains in $\Phi^{\text{QA}}(t)$, and thus, we still have a room to improve the method for the case that its value passes by 0 or π . We note that, for $\theta_L(0) = 0$ and π of SXS:BBH:0058, $\theta_L(t)$ also pass by 0 and π , respectively. However, the errors in phases are smaller than the cases in SXS:BBH:0037 and SXS:BBH:0164 because the precessing timescale is shorter and the interval staying close to 0 and π are shorter.

IV. DISCUSSION

In this paper, we proposed a new method for extracting the instantaneous orbital axis and for reconstructing the co-precessing waveforms from gravitational waves observed for generic precessing binary black holes. The

advantage of our method is as follows: Our method, at least in principle, enables us to extract the direction of the instantaneous orbital axis without assuming any model. In our method, we only made assumptions that $(l, m) = (2, \pm 2)$ modes of spherical harmonics in the co-precessing frame are the dominant modes in the strain and the time scales of the orbital precession and the gravitational-radiation reaction are much longer than the orbital period. Therefore, our method can be used even for the case that the orbit precesses in a way different from that general relativity predicts as far as these assumptions hold. The axis of the precession and the precessing frequency also provide us the information of the total angular momentum of the system for a single spinning binary. The amplitude and the phase of the co-precessing frame waveforms are also reconstructed without modeling their evolutions. Thus, using our method, the co-precessing frame waveforms are direct observables that can be constructed only from detector outputs. The parameter estimation from the precessing waveforms (and the non-precessing waveforms but observed from inclined direction) can be simplified by using the reconstructed co-precessing waveforms since the higher mode templates are not needed or, at least, less needed than using the inertia waveforms. Furthermore, the template models can become compact by using the approximate mapping between the co-precessing waveforms and non-precessing waveforms [36].

There are many other possible applications and extensions for our method. Our method can be extended to extract the higher modes in co-precessing frame, such as $m = 1$ and $m = 3$ components. In fact, we find that the co-precessing $(l, m) = (3, \pm 3)$ modes agree quite well with the wave components extracted from $|m| = 3$. The amplitude of $m = 1$ and $m = 3$ modes can be used to solve the degeneracy of parameter estimation between the symmetric mass ratio and the black-hole spin magnitude [3, 17, 25, 29]. Furthermore, our method can be applied to the data analysis of the waveforms from precessing black hole-neutron star mergers. The previous numerical studies [27, 28, 34, 38] pointed out that the location of the cutoff in the gravitational wave spectra (the cutoff frequency), caused by tidal disruption of neutron

stars, can be used to constrain the neutron star radius. However, the orbital precession (and the inclination of the observer) obscures the location of the cutoff by inducing the modulation in the spectra [21]. Since this problematic modulation is due to the mixing of the different wave components, the method we introduce in this work can be useful to remove such modulation, and may enable us to measure the cutoff frequency in the spectra using the reconstructed co-precessing waveforms [22]. These applications and extensions are now in progress.

In this paper, we assumed the situation that the complex wave strain is determined in sufficiently high accuracy, and hence, we neglect the effect of the noise and the error of the sky localization for simplicity, because our purpose is to demonstrate that the direct extraction of the orbital axis and the co-precessing frame waveforms is possible only from the information which we can obtain from the detection in principle. However, of course, data always suffer from the noise in reality. In particular, the sky localization error would be an important source of the error. We should test how well our method works in the presence of the noise and errors, and show what is the required signal-to-noise ratio for achieving the extraction in the required accuracy. Also, we need to extend our test to various models, for example, the case that the “transitional precession” occurs [8], since we only check the usefulness of our method in limited numbers of waveform models in this work.

ACKNOWLEDGMENTS

We are grateful to Andrea Taracchini for valuable discussion and checking the paper. We would like to thank the SXS Collaboration for freely providing a variety of high-precision gravitational waveforms of binary-black-hole coalescence. This work was supported by Grant-in-Aid for Scientific Research (Grant Nos. 24244028, 16K05347, 16H02183, 16H06342, 17H01131, 14J02950) of Japanese JSPS. Kyohei Kawaguchi was supported by JSPS Postdoctoral Fellowships for Research Abroad.

[1] <http://www.black-holes.org/waveforms>.

[2] <https://dcc.ligo.org/cgi-bin/DocDB/ShowDocument?docid=2974>.

[3] J. Aasi, J. Abadie, B. P. Abbott, R. Abbott, T. D. Abbott, M. Abernathy, T. Accadia, F. Acernese, C. Adams, T. Adams, and et al. Parameter estimation for compact binary coalescence signals with the first generation gravitational-wave detector network. *Phys. Rev. D*, 88(6):062001, September 2013.

[4] B. P. Abbott, R. Abbott, T. D. Abbott, M. R. Abernathy, F. Acernese, K. Ackley, C. Adams, T. Adams, P. Addesso, R. X. Adhikari, and et al. GW150914: The

Advanced LIGO Detectors in the Era of First Discoveries. *Physical Review Letters*, 116(13):131103, April 2016.

[5] B. P. Abbott, R. Abbott, T. D. Abbott, M. R. Abernathy, F. Acernese, K. Ackley, C. Adams, T. Adams, P. Addesso, R. X. Adhikari, and et al. GW151226: Observation of Gravitational Waves from a 22-Solar-Mass Binary Black Hole Coalescence. *Physical Review Letters*, 116(24):241103, June 2016.

[6] F. Acernese, M. Agathos, K. Agatsuma, D. Aisa, N. Allemandou, A. Allocca, J. Amarni, P. Astone, G. Balestri, G. Ballardin, and et al. Advanced Virgo: a second-generation interferometric gravitational wave detector.

- Classical and Quantum Gravity*, 32(2):024001, January 2015.
- [7] P. Amaro-Seoane, H. Audley, S. Babak, J. Baker, E. Barausse, P. Bender, E. Berti, P. Binetruy, M. Born, D. Boroluzzi, J. Camp, C. Caprini, V. Cardoso, M. Colpi, J. Conklin, N. Cornish, C. Cutler, K. Danzmann, R. Dolesi, L. Ferraioli, V. Ferroni, E. Fitzsimons, J. Gair, L. Gesa Bote, D. Giardini, F. Gibert, C. Grmani, H. Halloin, G. Heinzl, T. Hertog, M. Hewitson, K. Holley-Bockelmann, D. Hollington, M. Hueller, H. Inchauspe, P. Jetzer, N. Karnesis, C. Killow, A. Klein, B. Klipstein, N. Korsakova, S. L. Larson, J. Livas, I. Lloro, N. Man, D. Mance, J. Martino, I. Mateos, K. McKenzie, S. T. McWilliams, C. Miller, G. Mueller, G. Nardini, G. Nelemans, M. Nofrarias, A. Petiteau, P. Pivato, E. Plagnol, E. Porter, J. Reiche, D. Robertson, N. Robertson, E. Rossi, G. Russano, B. Schutz, A. Sesana, D. Shoemaker, J. Slutsky, C. F. Sopuerta, T. Sumner, N. Tamanini, I. Thorpe, M. Troebis, M. Vallisneri, A. Vecchio, D. Vetrugno, S. Vitale, M. Volonteri, G. Wanner, H. Ward, P. Wass, W. Weber, J. Ziemer, and P. Zweifel. Laser Interferometer Space Antenna. *ArXiv e-prints*, February 2017.
- [8] T. A. Apostolatos, C. Cutler, G. J. Sussman, and K. S. Thorne. Spin-induced orbital precession and its modulation of the gravitational waveforms from merging binaries. *Phys. Rev. D*, 49:6274–6297, June 1994.
- [9] K. G. Arun, A. Buonanno, G. Faye, and E. Ochsner. Higher-order spin effects in the amplitude and phase of gravitational waveforms emitted by inspiraling compact binaries: Ready-to-use gravitational waveforms. *Phys. Rev. D*, 79(10):104023, May 2009.
- [10] S. Babak, A. Taracchini, and A. Buonanno. Validating the effective-one-body model of spinning, precessing binary black holes against numerical relativity. *Phys. Rev. D*, 95(2):024010, January 2017.
- [11] J. Blackman, S. E. Field, M. A. Scheel, C. R. Galley, D. A. Hemberger, P. Schmidt, and R. Smith. A Surrogate Model of Gravitational Waveforms from Numerical Relativity Simulations of Precessing Binary Black Hole Mergers. *ArXiv e-prints*, January 2017.
- [12] L. Blanchet. Gravitational Radiation from Post-Newtonian Sources and Inspiraling Compact Binaries. *Living Reviews in Relativity*, 17:2, February 2014.
- [13] M. Boyle, L. E. Kidder, S. Ossokine, and H. P. Pfeiffer. Gravitational-wave modes from precessing black-hole binaries. *ArXiv e-prints*, September 2014.
- [14] M. Boyle, R. Owen, and H. P. Pfeiffer. Geometric approach to the precession of compact binaries. *Phys. Rev. D*, 84(12):124011, December 2011.
- [15] A. Buonanno, Y. Chen, and M. Vallisneri. Detecting gravitational waves from precessing binaries of spinning compact objects: Adiabatic limit. *Phys. Rev. D*, 67(10):104025, May 2003.
- [16] A. Buonanno, B. R. Iyer, E. Ochsner, Y. Pan, and B. S. Sathyaprakash. Comparison of post-Newtonian templates for compact binary inspiral signals in gravitational-wave detectors. *Phys. Rev. D*, 80(8):084043, October 2009.
- [17] H.-S. Cho, E. Ochsner, R. O’Shaughnessy, C. Kim, and C.-H. Lee. Gravitational waves from black hole-neutron star binaries: Effective Fisher matrices and parameter estimation using higher harmonics. *Phys. Rev. D*, 87(2):024004, January 2013.
- [18] R. Fernández and B. D. Metzger. Electromagnetic Signatures of Neutron Star Mergers in the Advanced LIGO Era. *Annual Review of Nuclear and Particle Science*, 66:23–45, October 2016.
- [19] M. Hannam, P. Schmidt, A. Bohé, L. Haegel, S. Husa, F. Ohme, G. Pratten, and M. Pürrer. Simple Model of Complete Precessing Black-Hole-Binary Gravitational Waveforms. *Physical Review Letters*, 113(15):151101, October 2014.
- [20] Ian Hinder et al. Error-analysis and comparison to analytical models of numerical waveforms produced by the NRAR Collaboration. *Class. Quant. Grav.*, 31:025012, 2014.
- [21] K. Kawaguchi, K. Kyutoku, H. Nakano, H. Okawa, M. Shibata, and K. Taniguchi. Black hole-neutron star binary merger: Dependence on black hole spin orientation and equation of state. *Phys. Rev. D*, 92(2):024014, July 2015.
- [22] Kyohei Kawaguchi. *Black Hole-Neutron Star Merger – Effect of Black Hole Spin Orientation and Dependence of Kilonova/Macronova–*. PhD thesis, Kyoto University, 3 2017.
- [23] S. Kawamura, M. Ando, N. Seto, S. Sato, T. Nakamura, K. Tsubono, N. Kanda, T. Tanaka, J. Yokoyama, I. Funaki, K. Numata, K. Ioka, T. Takahima, K. Agatsuma, T. Akutsu, K.-s. Aoyanagi, K. Arai, A. Araya, H. Asada, Y. Aso, D. Chen, T. Chiba, T. Ebisuzaki, Y. Ejiri, M. Enoki, Y. Eriguchi, M.-K. Fujimoto, R. Fujita, M. Fukushima, T. Futamase, T. Harada, T. Hashimoto, K. Hayama, W. Hikida, Y. Himemoto, H. Hirabayashi, T. Hiramatsu, F.-L. Hong, H. Horisawa, M. Hosokawa, K. Ichiki, T. Ikegami, K. T. Inoue, K. Ishidoshiro, H. Ishihara, T. Ishikawa, H. Ishizaki, H. Ito, Y. Itoh, K. Izumi, I. Kawano, N. Kawashima, F. Kawazoe, N. Kishimoto, K. Kiuchi, S. Kobayashi, K. Kohri, H. Koizumi, Y. Kojima, K. Kokeyama, W. Kokuyama, K. Kotake, Y. Kozai, H. Kunimori, H. Kuninaka, K. Kuroda, S. Kuroyanagi, K.-i. Maeda, H. Matsuhara, N. Matsumoto, Y. Michimura, O. Miyakawa, U. Miyamoto, S. Miyoki, M. Y. Morimoto, T. Morisawa, S. Moriwaki, S. Mukohyama, M. Musha, S. Nagano, I. Naito, K. Nakamura, H. Nakano, K. Nakao, S. Nakasuka, Y. Nakayama, K. Nakazawa, E. Nishida, K. Nishiyama, A. Nishizawa, Y. Niwa, T. Noumi, Y. Obuchi, M. Ohashi, N. Ohishi, M. Ohkawa, K. Okada, N. Okada, K. Oohara, N. Sago, M. Saijo, R. Saito, M. Sakagami, S.-i. Sakai, S. Sakata, M. Sasaki, T. Sato, M. Shibata, H. Shinkai, A. Shoda, K. Somiya, H. Sotani, N. Sugiyama, Y. Suwa, R. Suzuki, H. Tagoshi, F. Takahashi, K. Takahashi, K. Takahashi, R. Takahashi, R. Takahashi, T. Takahashi, H. Takahashi, T. Akiteru, T. Takano, N. Tanaka, K. Taniguchi, A. Taruya, H. Tashiro, Y. Torii, M. Toyoshima, S. Tsujikawa, Y. Tsunesada, A. Ueda, K.-i. Ueda, M. Utashima, Y. Wakabayashi, K. Yagi, H. Yamakawa, K. Yamamoto, T. Yamazaki, C.-M. Yoo, S. Yoshida, T. Yoshino, and K.-X. Sun. The Japanese space gravitational wave antenna: DECIGO. *Classical and Quantum Gravity*, 28(9):094011, May 2011.
- [24] L. E. Kidder. Coalescing binary systems of compact objects to (post)^{5/2}-Newtonian order. V. Spin effects. *Phys. Rev. D*, 52:821–847, July 1995.
- [25] A. Klein, P. Jetzer, and M. Sereno. Parameter estimation for coalescing massive binary black holes with LISA

- using the full 2-post-Newtonian gravitational waveform and spin-orbit precession. *Phys. Rev. D*, 80(6):064027, September 2009.
- [26] B. Kocsis, Z. Haiman, K. Menou, and Z. Frei. Pre-merger localization of gravitational-wave standard sirens with LISA: Harmonic mode decomposition. *Phys. Rev. D*, 76(2):022003, July 2007.
- [27] K. Kyutoku, H. Okawa, M. Shibata, and K. Taniguchi. Gravitational waves from spinning black hole-neutron star binaries: dependence on black hole spins and on neutron star equations of state. *Phys. Rev. D*, 84(6):064018, September 2011.
- [28] K. Kyutoku, M. Shibata, and K. Taniguchi. Gravitational waves from nonspinning black hole-neutron star binaries: Dependence on equations of state. *Phys. Rev. D*, 82(4):044049, August 2010.
- [29] R. N. Lang, S. A. Hughes, and N. J. Cornish. Measuring parameters of massive black hole binaries with partially aligned spins. *Phys. Rev. D*, 84(2):022002, July 2011.
- [30] Abdul H. Mroue et al. Catalog of 174 Binary Black Hole Simulations for Gravitational Wave Astronomy. *Phys. Rev. Lett.*, 111(24):241104, 2013.
- [31] Abdul H. Mroue and Harald P. Pfeiffer. Precessing Binary Black Holes Simulations: Quasicircular Initial Data. 2012.
- [32] R. O’Shaughnessy, B. Vaishnav, J. Healy, Z. Meeks, and D. Shoemaker. Efficient asymptotic frame selection for binary black hole spacetimes using asymptotic radiation. *Phys. Rev. D*, 84(12):124002, December 2011.
- [33] Y. Pan, A. Buonanno, A. Taracchini, L. E. Kidder, A. H. Mroué, H. P. Pfeiffer, M. A. Scheel, and B. Szilágyi. Inspiral-merger-ringdown waveforms of spinning, precessing black-hole binaries in the effective-one-body formalism. *Phys. Rev. D*, 89(8):084006, April 2014.
- [34] F. Pannarale, E. Berti, K. Kyutoku, B. D. Lackey, and M. Shibata. Gravitational-wave cutoff frequencies of tidally disruptive neutron star-black hole binary mergers. *Phys. Rev. D*, 92(8):081504, October 2015.
- [35] M Punturo, M Abernathy, F Acernese, B Allen, N Andersson, K Arun, F Barone, B Barr, M Barsuglia, M Beker, N Beveridge, S Birindelli, S Bose, L Bosi, S Braccini, C Bradaschia, T Bulik, E Calloni, G Cella, E Chassande Mottin, S Chelkowski, A Chincarini, J Clark, E Coccia, C Colacino, J Colas, A Cumming, L Cunningham, E Cuoco, S Danilishin, K Danzmann, G De Luca, R De Salvo, T Dent, R De Rosa, L Di Fiore, A Di Virgilio, M Doets, V Fafone, P Falferi, R Flaminio, J Franc, F Frasconi, A Freise, P Fulda, J Gair, G Gemme, A Genai, A Giazotto, K Glampedakis, M Granata, H Grote, G Guidi, G Hammond, M Hannam, J Harms, D Heinert, M Hendry, I Heng, E Hennes, S Hild, J Hough, S Husa, S Huttner, G Jones, F Khalili, K Kokeyama, K Kokkotas, B Krishnan, M Lorenzini, H Lück, E Majorana, I Mandel, V Mandic, I Martin, C Michel, Y Minenkov, N Morgado, S Mosca, B Mours, H Müller–Eberhardt, P Murray, R Nawrodt, J Nelson, R Oshaughnessy, C D Ott, C Palomba, A Paoli, G Parguez, A Pasqualetti, R Passaquieti, D Passuello, L Pinard, R Poggiani, P Popolizio, M Prato, P Puppò, D Rabeling, P Rapagnani, J Read, T Regimbau, H Rehbein, S Reid, L Rezzolla, F Ricci, F Richard, A Rocchi, S Rowan, A Rüdiger, B Sassolas, B Sathyaprakash, R Schnabel, C Schwarz, P Seidel, A Sintès, K Somiya, F Speirits, K Strain, S Strigin, P Sutton, S Tarabrin, A Thüring, J van den Brand, C van Leewen, M van Veggel, C van den Broeck, A Vecchio, J Veitch, F Vetranò, A Vicere, S Vyatchanin, B Willke, G Woan, P Wolfango, and K Yamamoto. The einstein telescope: a third-generation gravitational wave observatory. *Classical and Quantum Gravity*, 27(19):194002, sep 2010.
- [36] P. Schmidt, M. Hannam, and S. Husa. Towards models of gravitational waveforms from generic binaries: A simple approximate mapping between precessing and non-precessing inspiral signals. *Phys. Rev. D*, 86(10):104063, November 2012.
- [37] P. Schmidt, M. Hannam, S. Husa, and P. Ajith. Tracking the precession of compact binaries from their gravitational-wave signal. *Phys. Rev. D*, 84(2):024046, July 2011.
- [38] M. Shibata, K. Kyutoku, T. Yamamoto, and K. Taniguchi. Gravitational waves from black hole-neutron star binaries: Classification of waveforms. *Phys. Rev. D*, 79(4):044030, February 2009.
- [39] K. Somiya. Detector configuration of KAGRA—the Japanese cryogenic gravitational-wave detector. *Classical and Quantum Gravity*, 29(12):124007, June 2012.
- [40] R. Takahashi and T. Nakamura. The Decihertz Laser Interferometer Can Determine the Position of the Coalescing Binary Neutron Stars within an Arcminute a Week before the Final Merging Event to the Black Hole. *ApJL*, 596:L231–L234, October 2003.
- [41] A. Taracchini, A. Buonanno, Y. Pan, T. Hinderer, M. Boyle, D. A. Hemberger, L. E. Kidder, G. Lovelace, A. H. Mroué, H. P. Pfeiffer, M. A. Scheel, B. Szilágyi, N. W. Taylor, and A. Zenginoglu. Effective-one-body model for black-hole binaries with generic mass ratios and spins. *Phys. Rev. D*, 89(6):061502, March 2014.
- [42] The LIGO Scientific Collaboration, the Virgo Collaboration, B. P. Abbott, R. Abbott, T. D. Abbott, M. R. Abernathy, F. Acernese, K. Ackley, C. Adams, T. Adams, and et al. Binary Black Hole Mergers in the first Advanced LIGO Observing Run. *ArXiv e-prints*, June 2016.